Electrochemically-driven reduction of carbon dioxide mediated by mono-reduced Mo-diimine tetracarbonyl complexes: electrochemical, spectroelectrochemical and theoretical studies

Carlos Garcia Bellido, Lucia Álvarez-Miguel, Daniel Miguel, Noémie Lalaoui, Nolwenn Cabon, Frédéric Gloaguen, Nicolas Le Poul

ChemElectroChem

Articles
doi.org/10.1002/celc.202100359

Chemistry Europe
European Chemical
Societies Publishing

Electrochemically Driven Reduction of Carbon Dioxide Mediated by Mono-Reduced Mo-Diimine Tetracarbonyl Complexes: Electrochemical, Spectroelectrochemical and Theoretical Studies

Carlos Garcia Bellido,[a] Lucía Álvarez-Miguel,[a] Daniel Miguel,[b] Noémie Lalaoui,[a] Nolwenn Cabon,[c] Frédéric Gloaguen,*[a] and Nicolas Le Poul*[a]

The activation of carbon dioxide by three different Mo-diimine complexes [Mo(CO)$_4$(L)] (L=bipyridine (bpy), 1,10-phenantroline (phen) or pyridylindolizine (py-indz)) has been investigated by electrochemistry and spectroelectrochemistry. Under an inert atmosphere, monoreduction of the complexes is ligand-centered and leads to tetracarbonyl [Mo(CO)$_4$(L)]$^{\bullet-}$ species, whereas double reduction induces CO release. Under CO$_2$,

[Mo(CO)$_4$(L)] complexes undergo unexpected coupled chemical-electrochemical reactions at the first reduction step, leading to the formation of reduced CO$_2$ derivatives. The experimental results obtained from IR, NIR and UV-Vis spectroelectrochemistry, as well as DFT calculations, demonstrate an electron-transfer reaction whose rate is ligand-dependent.

1. Introduction

Extensive efforts towards the transformation of carbon dioxide into valuable fuels have been carried out during the last decades, achieving promising results by the development of photocatalytic,[1] electrocatalytic[2] and photoelectrochemical[3] devices. Molecular catalysts involving transition metals have been extensively investigated because metal-based systems are easily tunable and offer the possibility to directly rationalize the structure-reactivity relationships by simple variation of the ligand topology and/or the nature of the metal.[4] First molecular metal-based catalysts were predominantly developed with Ni[5] or Co[6] metal centers, and more heavy metals such as Re[7] or Ir.[8] This family of complexes was more recently

[a] C. Garcia Bellido, Dr. L. Álvarez-Miguel, Dr. N. Lalaoui, Dr. F. Gloaguen, Dr. N. Le Poul
Laboratoire de Chimie, Électrochimie Moléculaires et Chimie Analytique (UMR CNRS 6521)
Université de Bretagne Occidentale
6 Avenue Le Gorgeu, 29238 Brest, France
E-mail: frederic.gloaguen@univ-brest.fr
nicolas.lepoul@univ-brest.fr
[b] Prof. D. Miguel
GIR MIOMET-IU CINQUIMA, Química Inorgánica, Facultad de Ciencias
Universidad de Valladolid,
7 Paseo de Belén, 47011 Valladolid, Spain
[c] Dr. N. Cabon
ISCR (Institut des Sciences Chimiques de Rennes)
UMR 6226
F-35000 Rennes, France

supplanted by molecular catalysts based on more abundant and cheaper metals such as Mn[9] or Fe.[10] The two latter systems have been widely studied and still exhibit the best performances amongst reported molecular catalysts, although their uses as heterogeneous catalysts in aqueous media remain scarce.[11] In contrast, group 6 (Cr, Mo, W) metal-based systems have received less attention as homogeneous catalysts[4c,12] despite the presence of Mo and W centers in biological CO$_2$/CO processes.[13] Among them, metal-carbonyl derivatives bearing redox non-innocent 2,2'-bipyridine (bpy) ligands [M(CO)$_4$(bpy)] (M=Mo, W, Cr) have shown remarkable properties for the electrocatalytic CO$_2$ to CO transformation in terms of faradaic efficiency and turn-over frequency.[12k,m] However, the negative redox potential necessary to achieve electrocatalysis in organic solvents is still an obstacle to their prospective development as CO$_2$ catalysts. For instance, the proposed catalytic active species, [Mo(CO)$_3$(bpy)]$^{2-}$, is generated at $E=-2.7$ V vs. Fc$^+$/Fc in acetonitrile at a Pt or glassy carbon electrode, a potential value which is significantly more negative than those reported for analogous Mn or Fe complexes. Interestingly, recent works have demonstrated that a significant positive shift (up to 600 mV) of the catalytic potential could be achieved by using a gold electrode instead of Pt or carbon materials.[12j,m] Such enhancement was suggested to be due to interfacial processes favoring the formation of the tricarbonyl-reduced species [Mo-(CO)$_3$(bpy)]$^{\bullet-}$ and its electrochemical reduction at higher potential than usually found with Pt and C. Although modification of ligand topology by either introduction of adequate substituents on the backbone, or substitution by an analogous ligand is common in molecular electrocatalysis, this approach has been scarcely applied to molybdenum tetracarbonyl 2,2' bipyridine species for CO$_2$ reduction. So far, only [M(CO)$_4$(x,x'-R$_2$-bpy)] (x=x'=4, 5 or 6, R=Me, tBu, M=Mo, W) complexes were investigated, and their electrocatalytic properties were quite similar to the parent [M(CO)$_4$(bpy)] complex.[12k,l]

ChemElectroChem

Articles
doi.org/10.1002/celc.202100359

**Chemistry
Europe**
European Chemical
Societies Publishing

Alternatively, an unsymmetrical mono-imine molybdenum complex was shown to be reactive towards CO_2 when doubly-reduced. The resulting adduct featured C—C binding between CO_2 and the imine.[12f] More recently, Mo and W dipyridylamine (dpa) tetracarbonyl complexes showed an unexpected catalytic behavior at the mono-reduced state.[12c] DFT calculations suggested a strong ligand reorganization prior to reaction with CO_2.[12g]

In this context, we have focused our research on two analogues of the well-studied $[Mo(CO)_4(bpy)]$ catalyst (1), by considering the substitution of the bipyridyl ligand by 1,10 phenantroline (phen) or pyridylindolizine (py-indz) scaffolds, leading to $[Mo(CO)_4(phen)]$ (2) and $[Mo(CO)_4(py-indz)]$ (3) complexes, respectively (see Scheme 1). The choice of these two ligands was motivated by the possibility to rationalize the effect of rigid (phen) and unsymmetrical (py-indz) ligands on the electrochemical properties for CO_2 reduction, by comparison to the bpy parent complex 1. Meanwhile the synthesis and characterization of both complexes 2 and 3 were previously reported,[14] their reactivity towards CO_2 has never been explored. This paper thus reports the electrochemical, UV-Vis, near-IR and IR spectroelectrochemical studies of the reduction of three molybdenum complexes in organic media under inert and CO_2 atmosphere, together with DFT studies and chemical reduction experiments.

2. Results and Discussion

2.1. Synthesis and Solid-State Characterization

The complexes 1, 2 and 3 were prepared following previously described procedures and characterized by ^1H NMR and IR spectroscopy (see Supplementary Information).[14a,b,e,15] The solids were analyzed by solid state IR spectroscopy using an ATR detector. IR spectra for complexes 1, 2 and 3 displayed the characteristic four-signal pattern of tetracarbonyl diimine systems in the 1800–2050 cm^{-1} region, corresponding to $\nu(CO)$ frequency modes (Table S1).[16] Stretching energies did not significantly vary within the series, in agreement with X-ray data. The already-published XRD structures[14a,d,f] offer the possibility to analyze bond lengths and angles at solid state for 1, 2 and 3 (Tables S2 and S3). The three molybdenum complexes exhibit a pseudo-octahedral geometry centered on the metal atom, with two axial and two equatorial carbonyl ligands. X-ray data suggest a shorter Mo—C(O) axial bond for

complex 3 in comparison to complex 1 (Scheme 1). Moreover, whereas both Mo—N bond lengths are similar in the cases of 1 and 2, they are very different for 3. The shortest Mo—N bond is found for the nitrogen atom of the indolizine moiety, consistent with a better donation compared to pyridine.

2.2. Spectroscopic Characterization

^1H NMR, FTIR and UV-Visible spectroscopies were carried out for the characterization of the synthesized complexes in solution. NMR spectroscopy allowed accurate assignment of the hydrogen atoms of the bpy, phen, and py-indz groups in the aromatic region (7–8 ppm, see Supplementary Information). As found at solid state, IR spectroscopy in tetrahydrofuran (THF) displayed four main bands in the 1800–2050 cm^{-1} range corresponding to carbonyl stretching vibration modes (Figure 2, black curves). The values for the energy are somewhat similar to those found with solids, despite being up-shifted by 30 cm^{-1} for some frequency modes (Tables 1 and S1). This result suggests that while the pseudo-octahedral symmetry is preserved in THF, it is nevertheless varied due probable electrostatic interactions of the solvent with carbonyl groups.[14c] In particular, the lowest values of wavenumber were found for complex 3 as in solid state. Moreover, stretching energies for complexes 1 and 2 are similar to reported data in organic solvents.[16] UV-vis spectroscopy experiments exhibited several absorption bands in the 250–300 nm region assigned to π-π^* transitions within the diimine framework (Table 1). Electronic transitions at lower energies ($330 < \lambda < 490$ nm) result from $d(Mo) \rightarrow \pi^*(diimine)$ and $d(Mo) \rightarrow (CO_{ax})$ metal-to-ligand (MLCT) charge transfer transitions.[14c,16a,17] Noteworthy, the absorption band at ca. 470 nm for complexes 1 and 2 is blue-shifted by 25 nm for complex 3.
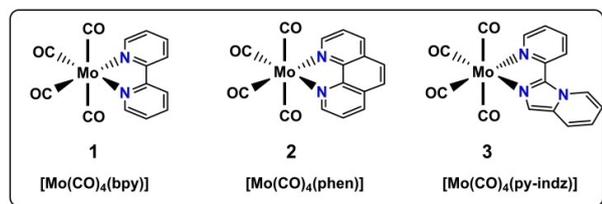
Scheme 1. Mo-diimine complexes 1, 2 and 3 studied for the electrochemically driven, CO_2 reduction and schematic atom numbering.

Table 1. UV-Vis (λ_{max}/nm) and IR (ν_{CO}/cm^{-1}) spectroscopic data for complexes 1, 2 and 3.[a]

Complex	λ_{max} [nm]	νCO [cm^{-1}]
$[Mo(CO)_4(bpy)]$ (1)	267, 297, 472	1840, 1880, 1900, 2012
$[Mo(CO)_4(phen)]$ (2)	263, 390, 469	1840, 1880, 1899, 2012
$[Mo(CO)_4(py-indz)]$ (3)	255, 340, 428	1836, 1877, 1895, 2010
$[Mo(CO)_4(bpy)]^{\bullet-}$	261, 297, 368, 497, 531, 854	1803, 1842, 1870, 1991
$[Mo(CO)_4(phen)]^{\bullet-}$	263, 284, 357, 564, 615, 832	1800, 1842, 1870, 1990
$[Mo(CO)_4(py-indz)]^{\bullet-}$	260, 345, 418, 595	1800, 1839, 1867, 1989
$[Mo(CO)_3(bpy)]^{2-}$	260, 369, 591, 638	1706, 1725, 1846
$[Mo(CO)_3(phen)]^{2-}$	264, 435, 634	1702, 1718, 1857
$[Mo(CO)_3(py-indz)]^{2-}$	261, 410, 662	1706, 1727, 1844

[a] Data obtained from spectroelectrochemical measurements in THF/ NBu_4PF_6 0.1 M.

ChemElectroChem

Articles
doi.org/10.1002/celc.202100359

**Chemistry
Europe**
European Chemical
Societies Publishing

2.3. Electrochemical and Spectroelectrochemical Characterization under Argon

Cyclic voltammetry experiments were performed in dry THF/ NBu_4PF_6 0.1 M at room temperature with a boron-doped diamond (BDD) working electrode. Similar results were obtained at a glassy carbon electrode (GC, see Figure S15). Electrochemical data are gathered in Table 2. First experiments were carried out under argon in order to decipher the chemically-

Table 2. Experimental electrochemical data (E / V vs. Fc^+/Fc) for complexes **1**, **2** and **3** (1 mM) in THF/NBu_4PF_6 0.1 M.

Complex	$E_{1/2}$ (1)	E_{pc}(2)
1	−1.85	−2.55
2	−1.90	−2.75
3	−2.20	−2.90
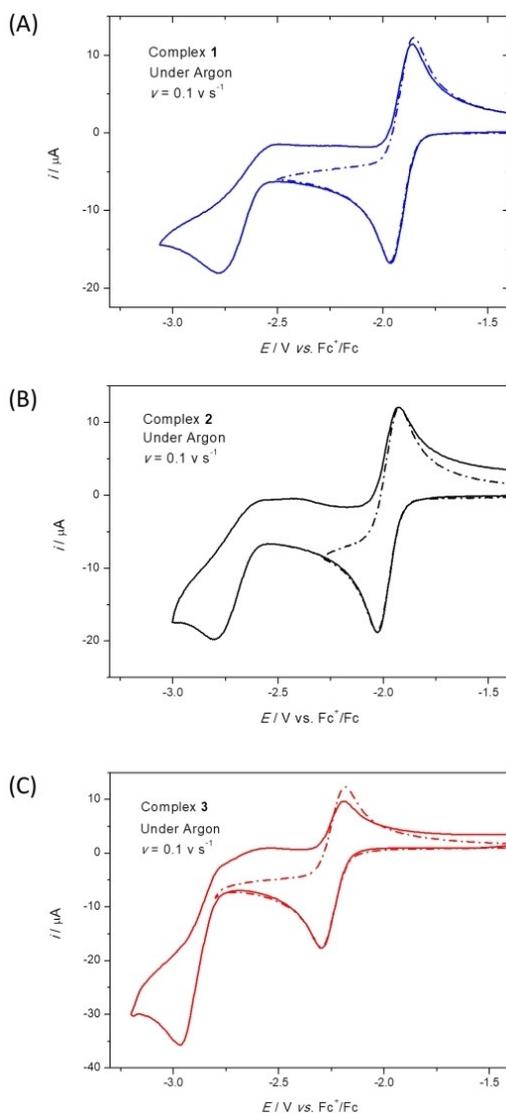
Figure 1. CVs at a BDD electrode (v = 0.1 V s^{-1}, E/V vs. Fc^+/Fc) of complexes **1** (Panel A), **2** (Panel B), and **3** (Panel C) in THF/NBu_4PF_6 0.1 M. C (complex) = 1 mM.

coupled reactions which can occur upon reduction. All complexes display two cathodic processes which can be ascribed to two successive monoelectronic reductions, according to previous studies on complex **1** (Figure 1).[12k,18] The first process occurring at $E_{1/2}$(1) (ca. −2.0 V vs. Fc^+/Fc, see Table 2) was reversible for all complexes (0.02 V s^{-1} < v < 1 V s^{-1}). Randles-Ševčik analysis (i_{pc}(1) vs. $v^{1/2}$, Figure S18) indicated that the first reduction is a diffusion-limited process. The formal potential varied with the nature of the diimine ligand, the most negative value being detected for complex **3**, as probably resulting from a stronger donating effect of the py-indz ligand (vs. phen and bpy). Further scanning towards more negative values led to the appearance of an irreversible cathodic peak at ca. E_{pc}(2) whose value varies with the ligand (Table 2). Increasing of the scan rate or decreasing of the temperature did not induce any better reversibility. Here, the doubly-reduced Mo complexes are unstable as tetracarbonyl species and undergo probable CO loss or protonation as previously suggested for complex **1**.[12k,m]

In-situ IR and UV-Vis spectroelectrochemistry (SEC) measurements were then carried out in order to identify the species generated during the reduction. An IR-SEC setup based on an ATR Si-probe in close contact to a glassy carbon conical electrode was designed for these experiments (Figure S8). It allowed in-situ probing of the redox species which were electrochemically generated within the thin layer separating the probe and the electrode surface. Potential-step methods such as chronoamperometry were preferred to low scan-rate CV for fast generation of these species. Typically, full transformation was obtained after 100 sec. of applied potential.

The Figure 2 displays the IR-SEC monitoring of both reduction processes for **1**, **2** and **3** under argon (subtracted from the solvent and electrolyte signature). For all complexes, the IR pattern obtained at the first reduction was typical of a tetracarbonyl molybdenum adduct, as previously reported for complex **1** (Figure 2, red curves).[12m] This is in agreement with the reversible redox behavior of the complexes at $E_{1/2}$(1), thus strongly suggesting the formation of the mononuclear [Mo-$(CO)_4(L)]^{•-}$ species (L = bpy, phen, py-indz). The shift of the four IR bands by ca. 30 cm^{-1} towards lower frequencies upon reduction is consistent with a lengthening of the CO bonds due to stronger back-bonding of the metal to the carbonyl moieties. It advocates for an increase of the electron density on the diimine ligand as well as on equatorial and axial CO moieties (see DFT studies, vide supra).[14c,19]

Investigation of the first reduction process was also carried out by in-situ time-resolved UV-Visible spectroelectrochemistry. New absorption bands at ca. 350–400 nm and 530–600 nm were detected (Figure S4), as previously found for mono-reduced metal-bound diimine species.[12l,m] Remarkably, low-energy broad bands were detected in the NIR region for **1**$^{•-}$, **2**$^{•-}$ and **3**$^{•-}$ (1200–2000 nm) (Figure S6). These bands may be ascribed to an intra-ligand charge-transfer transition and thus confirm the diimine character of the first cathodic process.[20] Further reduction of the complexes **1–3** until E_{pc}(2) under argon led to a modification of the IR and UV-Vis spectra. On one hand, the four v_{CO} bands found for the neutral and mono-reduced species evolved towards a 3-bands signature at ca. 1850 and

ChemElectroChem

Articles
doi.org/10.1002/celc.202100359

**Chemistry
Europe**
European Chemical
Societies Publishing
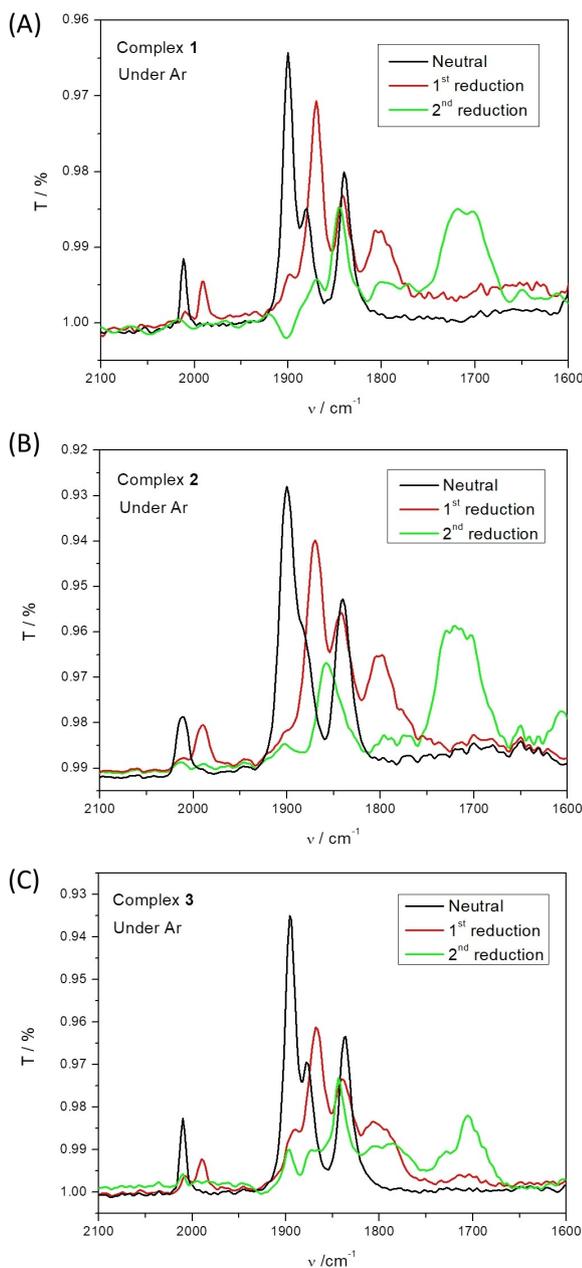
Figure 2. IR-SEC spectra of complexes **1** (Panel A), **2** (Panel B), and **3** (Panel C) in dry THF/NBu$_4$PF$_6$ 0.1 M under Ar. Black curve: neutral complexes; Red curve: after the 1st reduction; Green curve: after the second reduction.

1700 cm^{-1} (Figure 2, green curves, and Table 1). Such a behavior was previously described for the bpy-Mo complex and is diagnostic of a tricarbonyl molybdenum-diimine species, namely [Mo(CO)$_3$(L)]$^{2-}$. On the other hand, UV-Vis spectroelectrochemical measurements showed the appearance of broad peaks centered at $\lambda_{max}=638$, 634 and 662 nm for complexes **1**, **2** and **3**, respectively (Figure S4). Moreover, the double-reduction was accompanied with the disappearance of the 1200–2000 nm NIR band found for the complexes (Figure S6). The latter result hence suggests that injection of a second electron induces the loss of electronic delocalization on the diimine backbone.

Thus, experimental data clearly indicate that electrochemical reduction under argon induces the same processes for the three complexes, independently of the nature of the diimine ligand i.e. (i) a monoelectronic reduction leading to the formation of a tetracarbonyl [Mo(CO)$_4$(L)]$^{\bullet-}$ species whose spin density is essentially localized on the diimine scaffold and (ii) a bi-electronic reduction yielding a tricarbonyl [Mo(CO)$_3$(L)]$^{2-}$ species with rapid loss of one CO ligand in dry THF.
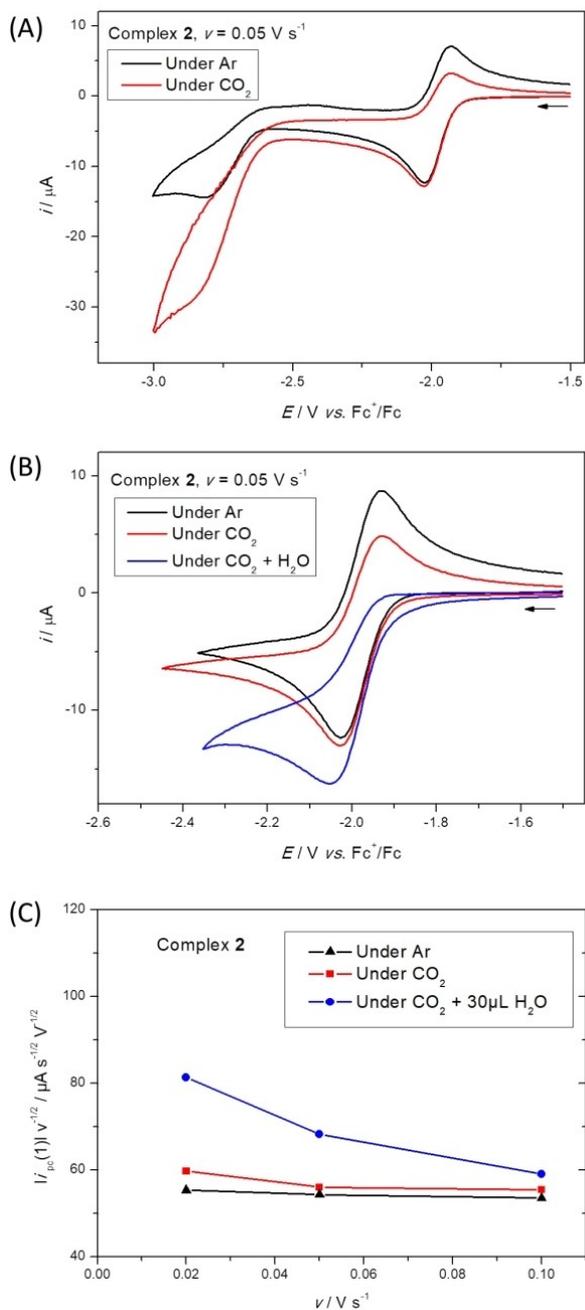
2.4. Electrochemical and Spectroelectrochemical Characterization under CO$_2$

Electrochemical properties of the complexes **1**–**3** were then investigated in a CO$_2$-saturated THF/NBu$_4$PF$_6$ 0.1 M solution. BDD or glassy carbon working disc electrodes were preferred to metal (Pt, Au) materials in order to avoid direct CO$_2$ electro-reduction given the negative values of $E_{pc}(2)$ for complexes **1**–**3**, or surface-mediated effects.[12j,m] Cyclic voltammetry was first carried out in dry THF. At $v=0.1$ V s^{-1}, complexes **1** and **2** did not exhibit any significant increase of the peak current $i_{pc}(1)$ or shift of $E_{pc}(1)$ (Figure S13A and B) in contrast to complex **3** (Figure S13C). Moreover, on this first reduction system, complexes **2** and **3** displayed a loss of reversibility (total loss for **3**) whereas CV of complex **1** was the same as under Ar.

At more negative potential values, two different redox behaviors were found depending on the nature of the diimine ligand. For complexes **1** and **2**, a significant increase of the peak current at $E_{pc}(2)$ was observed (Figure S13A and B), which likely corresponds to the reaction of CO$_2$ with [Mo(CO)$_3$(L)]$^{2-}$.[12k,m] In contrast, for the complex **3**, two broad and undefined peaks of low intensity were detected at potential values ranging between $E_{pc}(1)$ and $E_{pc}(2)$ (Figure S13C), whereas the peak at $E_{pc}(2)$ was no longer identified.

Lowering the scan rate was shown to have a significant effect on the first reduction process. Indeed, a substantial increase of the peak current at $E_{pc}(1)$ and a loss of reversibility were observed as compared to the dry conditions, as shown in Figure 3B for complex **2** at $v=0.05$ V s^{-1} (red curve). Under strictly identical conditions, this current increase was higher for complexes **2** and **3** than for complex **1**, as shown by plots of the current function $i_{pc}(1)$ $v^{-1/2}$ against v under Ar and CO$_2$ (red curve in Figure 3C for complex **2**, and Figure S14 for complexes **1** and **3**). Addition of aliquots of water under CO$_2$ was accompanied by an increase of the peak current (Figures 3B–C, S14 and S17). A maximum peak current value was obtained after addition of ca. 0.1% H$_2$O (vol.). Control experiments revealed no effect of water on the peak potential or current at this redox potential under argon (Figure S16).

In order to better quantify the observed electrochemical changes at the mono-reduced state for complexes **1** and **2**, simulation of the experimental CVs was carried out by using a voltammetric simulator package (see Supplementary Information). Only a EC$_{cat}$ mechanism (E = electrochemical, C = chemical) was considered since IR spectroscopic studies with chemically-reduced complexes showed the back generation of the neutral complexes **1**–**3** by reaction with CO$_2$ (vide supra), hence

ChemElectroChem

Articles
doi.org/10.1002/celc.202100359

Chemistry
Europe
European Chemical
Societies Publishing

Figure 3. CVs (E/V *vs.* Fc^+/Fc) at a BDD working electrode of complex **2** (1 mM), in dry THF/NBu$_4$PF$_6$ 0.1 M; Panel A: For $v = 0.05$ V s^{-1} under argon (black) and CO$_2$ (red); Panel B: For $v = 0.05$ V s^{-1} under argon (black), under CO$_2$ (red), and under CO$_2 + 0.1\%$ H$_2$O (v) (blue); Panel C: Plots of |$i_{pc}(1)$| $v^{-1/2}$ against v under Ar (black), under CO$_2$ (red), and under CO$_2 + 0.1\%$ H$_2$O (blue).

the forward and the backward rate constants (see Supplementary Information). Although these data have to be taken with caution, they support the hypothesis that the ligand topology impacts the electron transfer kinetics for CO$_2$ conversion at the first reduction step. This redox behavior is reminiscent to that observed for Mo and W tetracarbonyl dipyridylamine (dpa) complexes which underwent substantial current increase at the first reduction step after strong ligand reorganization.[12c,g] However, in our case, IR- and UV-Vis-SEC of complexes **1**–**3** under Ar were not indicative of any specific conformational change upon monoelectronic reduction.

Bulk electrolysis experiments under CO$_2$ followed by analysis of the gaseous products by chromatography was not conducted (see experimental section). However, aiming at better rationalizing this discrepancy and qualitatively analyze the products of the reaction, IR and UV-Vis-NIR spectroelectrochemical studies were performed under CO$_2$ for the three complexes. As shown in Figure 4A, the electrochemical reduction under CO$_2$ of complex **1** led to the appearance of ν_{CO} bands typically
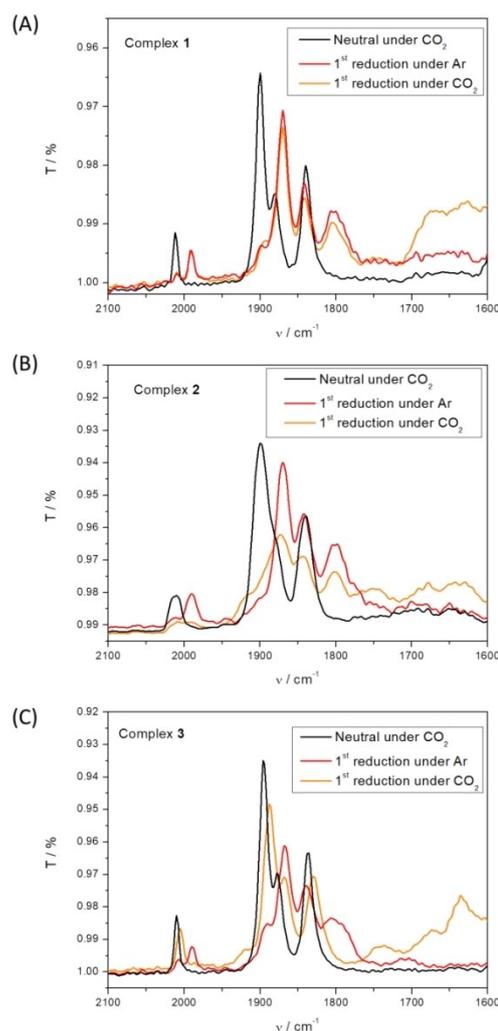
Figure 4. IR-SEC spectra of complexes **1** (Panel A), **2** (Panel B), and **3** (Panel C) in dry THF/NBu$_4$PF$_6$ 0.1 M before (black) and after (orange) reduction at $E_{1/2}(1)$ under CO$_2$. For comparison, IR spectra after reduction at $E_{1/2}(1)$ under Ar (red) are given.

discriminating an ECE process (which would have not led back to the neutral species) or an EC process (which would have induced a minor (10%) increase of the peak current).[21] The experimental curves obtained under Ar and CO$_2$ at $v = 0.05$ V s^{-1} (with and without added water) for the two complexes were satisfactorily reproduced by varying kinetics of the chemical reaction (Figure S19). Interestingly, the cathodic peak current value behavior appeared as mainly controlled by both

ChemElectroChem

Articles
doi.org/10.1002/celc.202100359

Chemistry Europe
European Chemical
Societies Publishing

ascribed to the mono-reduced tetracarbonyl species [M-$(CO)_4(bpy)]^{•-}$ ($1^{•-}$). The same conclusion could be drawn for complex **2**, except that only low intensity bands featuring $2^{•-}$ were found (Figure 4B). The complex **3** did not exhibit any IR response corresponding to $3^{•-}$ but rather a new spectrum typical of a tetracarbonyl Mo species (Figure 4C). In addition, all complexes showed supplementary bands (not observed under argon, see red curves in Figure 4) in the 1550–1700 cm^{-1} region, which were ascribed to carbonate and formate ions as previously reported,[12l,22] and in agreement with our control experiments (Figure S11). Further IR measurements also demonstrated that these bands were not detected at the resting potential of the neutral species (see for instance Figure S12 for complex **2**), thus showing the need for electron source. Furthermore, IR-SEC experiments performed in the dark yielded similar results to those carried out in daylight, thus excluding a photoactivated process. Noteworthy, complexes **2** and **3** displayed two new bands at 1920 and 1750 cm^{-1}, which were previously reported for the electrocatalytic reduction of CO_2 by Mo-diimine complexes.[12e,m] The amplitude of these supplementary bands was shown to increase with water content.

UV-Vis spectroelectrochemistry was also carried out for CO_2 reactivity for the first reduction process, revealing the presence of the mono-reduced species $1^{•-}$ and $2^{•-}$ (partially) whereas the complex $3^{•-}$ was not identified, in agreement with IR data (Figure S5). NIR-spectroelectrochemistry was also consistent with IR and UV-Vis spectroscopic results since low-energy intraligand charge transfer absorption bands detected under argon were no longer observed for complexes **2** and **3** under CO_2, whereas it remained the same for complex **1** (Figure S7). Thus, this clearly evidences that mono-reduced species $2^{•-}$ and $3^{•-}$ reacted instantly with CO_2.

2.5. Chemical Generation and Reactivity versus CO_2 of Mono- and Bis-Reduced Species

In complement to spectroelectrochemical studies, mono-reduced complexes were prepared by reacting complexes **1**–**3** with one equivalent of chemical reductant KC_8 in THF under argon. The resulting complexes displayed similar IR signatures to those found by spectroelectrochemistry (Figure S10, red curves), thus confirming the formation of tetracarbonyl species $1^{•-}$, $2^{•-}$ and $3^{•-}$. Reaction of the mono-reduced species with carbon dioxide was monitored by IR spectroscopy (Figure S10). For all complexes, the resulting spectra indicated the back and partial generation of the neutral complexes **1**–**3**, together with new species displaying stretching bands in the 1600–1750 cm^{-1} region, which can be ascribed to C–O vibrations of bicarbonate and formate anions as seen by IR-SEC.[12l,22] Noteworthy, formation of these new species was revealed to be significantly accelerated in presence of 0.1% water in dry THF. These results evidenced the participation of protons/water to CO_2 reduction by the mono-reduced Mo complexes in good agreement with electrochemical and spectroelectrochemical data.

2.6. DFT Calculations

A series of DFT calculations were performed in order to get insights into the reaction of the mono-reduced species with CO_2. Preliminary calculations allowed the determination the standard potential of the $[CO_2]^{0/•-}$ couple. The resulting value (-2.85 V vs. $Fc^{+/0}$) was at least 0.8 V more negative than those of $[Mo(CO)_4L]^{0/•-}$, thus ruling out the possibility of CO_2 activation at the mono-reduced state through an outer sphere electron transfer (no bond making/cleavage). From this result, we investigated a catalytic mechanism in which CO_2 is activated by its association with a reduced form of the complexes possessing a vacant site, i.e. $[Mo(CO)_3(L)]^{•-}$ according to previous studies.[12j,m]

A series of geometry optimization was performed for the three different binding modes of CO_2 that have been reported in mononuclear transition metal complexes, i.e. η^1-OCO, η^1-CO_2 and η^2-CO_2.[2d] Formation of a η^1-OCO adduct and subsequent protonation of the C atom is thought to favor the production of formate, one of the products detected by IR-SEC experiments.[2d] However, for all complexes, geometry optimization starting with a CO_2 ligand bound in the η^1-OCO mode did not converged to a stable structure. On the other hand, when starting with a CO_2 ligand bound in the η^1-CO_2 mode, structures in which the CO_2 ligand can adopt a η^2-CO_2 binding mode were obtained (Figure 5A).

Relevant bond distances and angles are listed in Table S5. In the CO_2 adducts, the O–C–O angle is the range 141–143°, close to the value of 135° calculated for an isolated $[CO_2]^{•-}$ radical anion. Besides, the C–O bonds are elongated by 0.04–0.07 Å as

(A)

$[Mo(CO)_3(phen)(CO_2)]^{•-}$

(B)
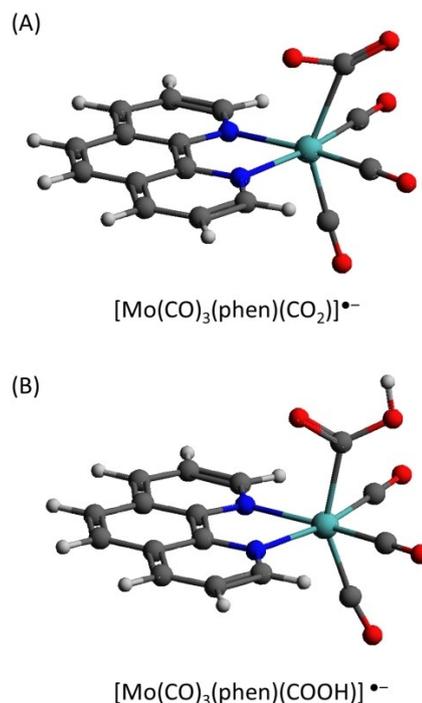
$[Mo(CO)_3(phen)(COOH)]^{•-}$

Figure 5. Calculated structures of (A) $[Mo(CO)_3(phen)(CO_2)]^{•-}$ and (B) $[Mo(CO)_3(phen)(COOH)]^{•-}$. Atom colors: H (white), C (grey), N (blue), O (red) and Mo (green).

ChemElectroChem

Articles
doi.org/10.1002/celc.202100359

Chemistry
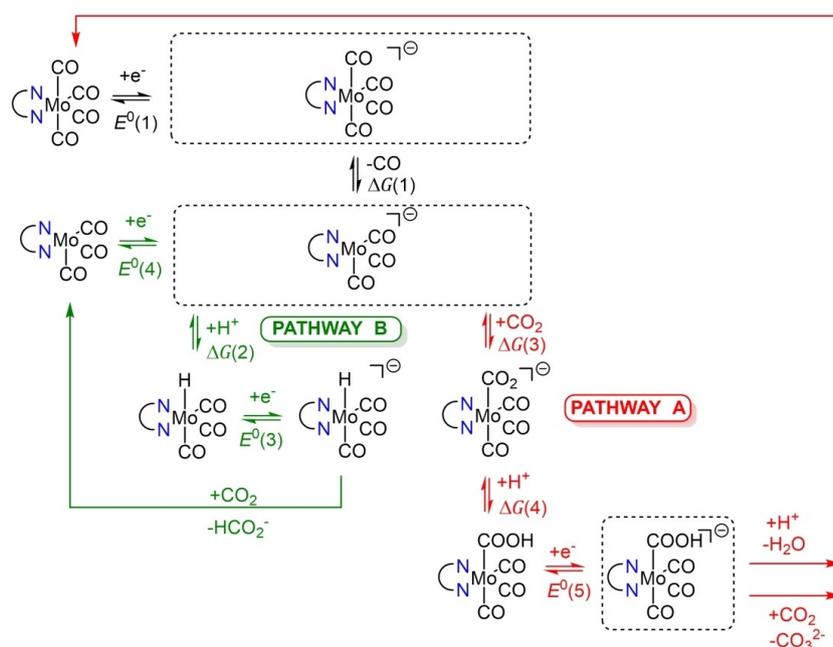**Europe**
European Chemical
Societies Publishing

compared to those in an isolated CO_2 molecule, indicative of a weakening of the bond strength. These geometric features clearly demonstrate a significant transfer of electronic density from the $[Mo(CO)_3(L)]^{\bullet-}$ moiety to the bound CO_2 (*vide infra*).

Our next set of analyses was hence devoted to the calculations of the redox potentials of the electron transfer steps and of the free energies of the chemical steps involved in the formation and reactivity of CO_2 adducts. The resulting thermodynamic data are gathered in Table 3. Starting from $[Mo(CO)_4(L)]^{\bullet-}$, the CO loss is uphill in energy by $\Delta G(1) = +26.7$, $+26.4$ and $+24.9$ kcal mol^{-1} for L=bpy, phen and py-indz, respectively (Schemes 2 and 3, and Table 3). Two different situations may be then considered.

The first one includes the binding of CO_2 to $[Mo(CO)_3(L)]^{\bullet-}$, yielding the corresponding $[Mo(CO)_3(L)(CO_2)]^{\bullet-}$ adduct according to Pathway A (Scheme 2). This reaction was recently discussed in the frame of DFT studies for a series metal-bipyridine tetracarbonyl complexes.[12d] This process is slightly downhill in energy ($\Delta G(3) = -2.4$, -2.4 and -2.6 kcal mol^{-1} for L=bpy, phen and py-indz, respectively (see Table 3)). The next

Table 3. Theoretical data correlated to the mechanistic pathways depicted in Scheme 2. E^0 in V *vs.* Fc$^+$/Fc; ΔG in kcal.mol^{-1}.
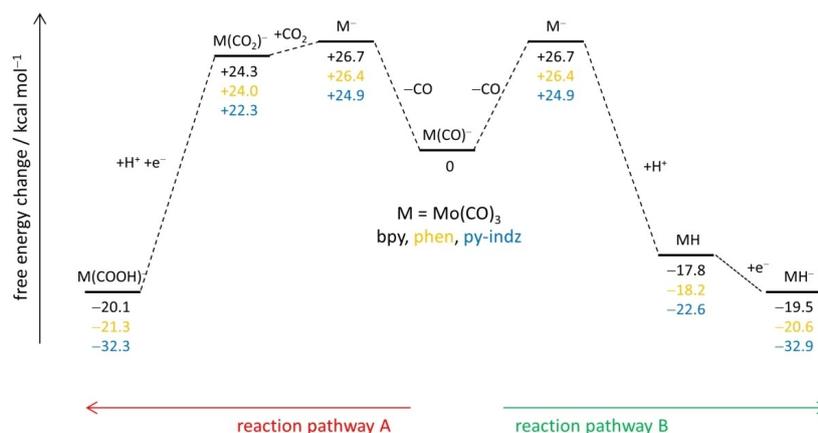
| Complex	1	2	3
$E^0(1)$	−1.85	−1.88	−2.16
$E^0(3)$	−0.90	−0.91	−0.99
$E^0(4)$	−1.57	−1.58	−1.81
$E^0(5)$	−0.71	−0.72	−0.80
$\Delta G(1)$	+26.7	+26.4	+24.9
$\Delta G(2)$	−17.8	−18.2	−22.8
$\Delta G(3)$	−2.4	−2.4	−2.6
$\Delta G(4)$	−18.1	−18.1	−23.5

Scheme 2. Suggested mechanistic pathways for the CO_2 reduction mediated by Mo-diimine complexes **1**, **2** and **3**.

Scheme 3. Energy profile for the CO_2 reduction mediated by Mo-diimine complexes **1**, **2** and **3** for the reactions pathways A and B.

ChemElectroChem

Articles
doi.org/10.1002/celc.202100359

Chemistry
Europe
European Chemical
Societies Publishing

step is most likely the protonation of the CO_2 ligand even in the absence of added proton source (residual water in the medium may be sufficient to trigger the reaction). Since production of formate was detected by IR-SEC experiments, we first considered that protonation could occur at the C atom of the CO_2 ligand according to this pathway. However, all attempted calculations aimed at optimizing the geometry of such intermediates failed to converge. On the other hand, protonation at the O atom of the CO_2 ligand was found to be downhill in energy as shown by the values of $\Delta G(4)$ in Table 3. Summing values of $\Delta G(1)$, $\Delta G(3)$ and $\Delta G(4)$ indicated that the reaction $[Mo(CO)_4(L)]^{\bullet-} + CO_2 + H^+ \rightarrow [Mo(CO)_3(L)(COOH)] + CO$ following pathway A is uphill in energy by $+6.2$ and $+5.4$ kcal mol^{-1} for L=bpy and phen, while slightly downhill in energy by -1.2 kcal mol^{-1} for L=py-indz. In addition, the calculated reduction potentials $E^0(5)$ of the $[Mo(CO)_3(L)(COOH)]$ intermediates are significantly less negative than the reduction potential of the $[Mo(CO)_4(L)]$ complexes (by ca. 1.2 V, see Table 3). This result implies that the protonation step of the $[Mo(CO)_3(L)(CO_2)]^{\bullet-}$ adducts is immediately followed by a reduction step leading to $[Mo(CO)_3(L)(COOH)]^{\bullet-}$ (see Figure 5B for the phen derivative). Structure calculations showed that subsequent protonation of these negatively charged intermediates leads to $C-O(H)_2$ bond cleavage releasing H_2O and regenerating $[Mo(CO)_4(L)]$ which is electrochemically reduced into $[Mo(CO)_4(L)]^{\bullet-}$ at $E^0(1)$ (see Figure 6A for the phen derivative). The conversion of CO_2 into CO and H_2O activated by the reduction of $[Mo(CO)_4(L)]$ complexes has thus an overall driving force of -20.1, -21.3 and -32.3 kcal mol^{-1} for L=bpy, phen and py-indz, respectively (Scheme 3). The driving force is noticeably larger for L=py-indz, which can be explained by a more negative reduction potential value for this derivative. We did not calculate the activation barriers of the chemical steps described above. However, the detection of $[Mo(CO)_4(L)]^{\bullet-}$ intermediates under inert atmosphere by IR-SEC experiments indicates that the activation barrier of the CO loss to give $[Mo(CO)_3(L)]^{\bullet-}$ must be significantly larger than that of the first protonation step of bound CO_2.

The second situation that we have considered is the direct protonation of the $[Mo(CO)_3(L)]^{\bullet-}$ intermediate according to Pathway B in Scheme 2. Such a possibility was envisaged because Pathway A cannot support the generation of formate, in contrast to what is observed experimentally. Formation of hydride-Mo carbonyl complexes was previously reported, but resulting from the reaction of the bis-reduced $Mo(CO)_6$ species with protons.[12h] According to Pathway B, the formation of the corresponding hydride derivatives $[Mo(CO)_3(L)(H)]$ is downhill by $\Delta G(2) = -17.8$, -18.2 and -22.8 kcal mol^{-1} for L=bpy, phen and py-indz, respectively. In addition, the reduction potential $E^0(3)$ of these hydrides is significantly less negative (by ca. 1.0 V, see Table 3) than $E^0(1)$. This result implies that the protonation of $[Mo(CO)_3(L)]^{\bullet-}$ is immediately followed by a reduction step leading to $[Mo(CO)_3(L)(H)]^{\bullet-}$. Structure calculations showed that the reaction of these reduced hydrides with CO_2 leads to Mo–H bond cleavage leading to formate and $[Mo(CO)_3(L)]$ (Figure 6B), the latter being immediately reduced back to $[Mo(CO)_3(L)]^{\bullet-}$ at $E^0(4)$ (see Table 3). Overall, the production of formate by the
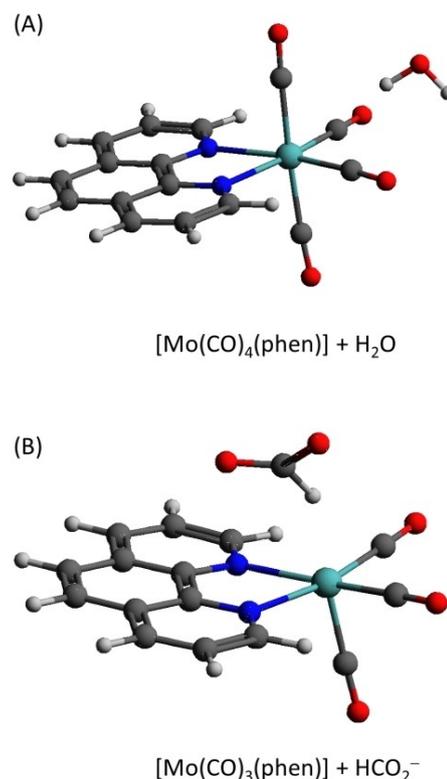
Figure 6. Calculated structures (A) upon protonation of $[Mo(CO)_3(phen)(COOH)]^{\bullet-}$ leading to the release of water and generation of $[Mo(CO)_4(phen)]$ according to Pathway A, and (B) reaction of $[Mo(CO)_3(phen)(H)]^{\bullet-}$ with CO_2 leading to the release of formate and $[Mo(CO)_3(phen)]$ according to pathway A. Atom colors: H (white), C (grey), N (blue), O (red) and Mo (green).

reduction of $[Mo(CO)_4(L)]$ in the presence of CO_2 and a proton source has thus a driving force of -19.5, -20.6 and -32.9 kcal mol^{-1} for L=bpy, phen and py-indz, respectively (Scheme 3). These free energy values are comparable to those calculated for the production of CO and H_2O according to Pathway A (*vide infra*) (Scheme 3). The mechanism leading to the production of formate should however be favored in the presence of added water, which is what was observed experimentally. In addition, once initiated, this mechanism bypasses the CO loss reaction $[Mo(CO)_4(L)]^{\bullet-} \rightarrow [Mo(CO)_3(L)]^{\bullet-} + CO$. However, the protonation of the metal center in $[Mo(CO)_3(L)]^{\bullet-}$ yielding a $[Mo(CO)_3(L)(H)]$ hydride has most likely a higher energy barrier than the protonation of the partly reduced bound CO_2 in $[Mo(CO)_3(L)(CO_2)]^{\bullet-}$, which might explain the low catalytic activity experimentally measured.

Generation of CO_3^{2-} ions is generally explained by the reaction of a transient reduced metal-CO_2 adduct with a supplementary carbon dioxide molecule,[12g,23] leading to C–O bond cleavage and release of bicarbonate while a carbonyl ligand remains attached to the metal ion (Scheme 2). According to DFT studies, the binding of a supplementary CO_2 molecule to $[Mo(CO)_3(L)(COOH)]^{\bullet-}$ yields a stable $[Mo(CO)_3(L)(COOH)(CO_2)]^{\bullet-}$ adduct (see Figure S21 for L=phen) through a thermodynamically uphill process ($\Delta G = +13.8$ kcal mol^{-1} for L=phen). Another possible explanation for carbonate production during

ChemElectroChem

Articles
doi.org/10.1002/celc.202100359

**Chemistry
Europe**
European Chemical
Societies Publishing

electroreduction can be the reductive disproportionation of CO_2 into carbonate and CO, which usually occurs in presence of Lewis acids such as Mg^{2+} or other metal ions.[2d,9b,24] Alternatively, the acid-base equilibria $CO_2 + H_2O \rightarrow H^+ + HCO_3^-$ and $CO_2 + H_2O \rightarrow 2H^+ + CO_3^{2-}$ may also explain the increase of carbonates content since pathway A favors the formation of water. This assumption is supported by DFT calculations, which show that protonation of $[Mo(CO)_3(L)(CO_2)]^{\bullet-}$ by displacement of the dioxide-carbonate acid-base equilibrium and further reduction of the protonated intermediates at $E^0(1)$ has an overall driving force of -13.5, -14.3 and -23.8 kcal mol^{-1} for for L=bpy, phen and py-indz, respectively (Table S11). Moreover, the protonation and further reduction of $[Mo(CO)_3(L)]^{\bullet-}$ following the same pathway has an overall driving force of -8.6, -9.5 and -18.8 kcal mol^{-1} for for L=bpy, phen and py-indz, respectively (Table S12).

2.7. Electronic Structures

To gain insight on the localization of the electronic density in the catalytic intermediates, we first analyzed selected bond lengths and angles of the calculated structures (Tables S5–S7). For all complexes, calculated structures were optimized starting from X-ray data at neutral state by including a dielectric continuum to model the electrolyte (see experimental section for details).

The calculated structures of the tetracarbonyl complexes $[Mo(CO)_4(L)]$ display bond distance and bond angle values that are in good agreement with those determined from the X-ray data. Noteworthy, the two Mo–N bond lengths are sensibly different in $[Mo(CO)_4(py\text{-}indz)]$ (2.285 and 2.238 Å, respectively), in contrast to the bpy and phen derivatives in which they are strictly identical (Tables S6 and S7). The shortening of one of the two Mo–N bonds depicts the better electron donating property of the indolizine vs. pyridyl moiety and an unsymmetrical charge location. The structures of the reduced tetracarbonyl intermediates $[Mo(CO)_4(L)]^{\bullet-}$ are similar to those of the corresponding neutral complexes (Tables S6 and S7). Electron input induces a slight increase of the C–O and Mo–N bond lengths, as well as a shortening of Mo–C(O) bonds. Moreover, a significant decrease of the (N)C–C(N) bond length by 0.030–0.045 Å was found, hence indicating that the π* orbital of the non-innocent ligands L is occupied. These results are in line with spectroelectrochemical data which suggest a stronger back-bonding of Mo to the CO ligands, and an increase of the electron density on the diimine ligand. The 30 cm^{-1} IR shift of the four carbonyl stretching bands which was detected by IR-SEC was nicely reproduced for the three complexes (Figure S20 and Table S8), thus confirming the good matching of the mono-reduced model with the experimental data.
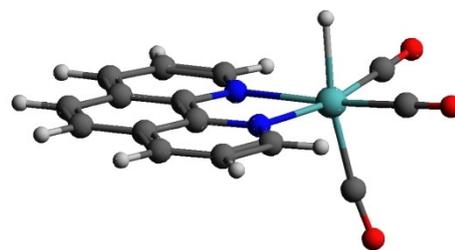
The calculated structures of the $[Mo(CO)_3(L)]^{\bullet-}$ intermediates show that the departure of a CO ligand opens a vacant site in axial position. The CO loss induces a substantial shortening of the axial Mo–CO bond together with that of the two Mo–N bonds (Table S6). This is accompanied by an increase of the angle between the axial CO and the Mo-diimine moiety from

ca. 93° to 107°. The CO loss yields thus a twist of the diimine ligand towards the axial vacant site, emphasizing a distortion from the ideal square-based pyramidal geometry. Besides, a slight but noticeable lengthening of the (N)C–C(N) bond was found suggesting that some electronic density has been transferred from the π* orbital of the diimine ligand to the Mo(CO)$_3$ moiety (vide infra).

Additional calculations were carried out on the $[Mo(CO)_3(L)(CO_2)]^{\bullet-}$ adducts proposed for the Pathway A. Theoretical structures show evidence for a transfer of electronic density to the CO_2 ligand (vide infra). However, the (N)C–C(N) bond lengths are quite similar in $[Mo(CO)_3(L)]^{\bullet-}$ and $[Mo(CO)_3(L)(CO_2)]^{\bullet-}$ suggesting that the electronic density is mostly transferred from the Mo(CO)$_3$ moiety (Tables S5 and S6). Interestingly, the $[Mo(CO)_3(L)(CO_2)]^{\bullet-}$ and $[Mo(CO)_3(L)(COOH)]^{\bullet-}$ complexes display significant structural differences (Figure 5, Tables S5–S7). The Mo–C(OOH) bond is indeed shorter than the Mo–C(O$_2$) bond by 0.070–0.084 Å, indicating a stronger Mo–C binding. In the meantime, the C–O(H) bond is longer than the C–O bond by 0.19 Å, evidencing a weakening of the C–O bond strength. Importantly, the (N)C–C(N) bond in $[Mo(CO)_3(L)(COOH)]^{\bullet-}$ is elongated by 0.019–0.030 Å compared to this bond in $[Mo(CO)_3(L)(CO_2)]^{\bullet-}$, indicating less electronic density in π* orbital of the L ligands. These observations are consistent with a transfer of electronic density from the diimine moiety to the COOH ligand which may favor C–O bond cleavage and water formation.

Electronic structures of $[Mo(CO)_3(L)(H)]^{\bullet-}$ were also calculated to better investigate the Pathway B (see Figure 7 for the phen derivative structure). The Mo–H bond lengths are in the range 1.84–1.85 Å (Table S9). Compared to their respective values in $[Mo(CO)_4(L)]^{\bullet-}$, the Mo–N bonds are shorter and the (N)C–C(N) bond is longer in the reduced metal hydrides, consistent with a transfer of electronic density from the diimine moiety to the hydride ligand, thus activating the site for further reaction with carbon dioxide.

To complement the analysis of the structures, we now discuss the Mulliken charges for several catalytic intermediates listed in Table S10. On the average, in $[Mo(CO)_3(L)]^{\bullet-}$, the Mo center carries a positive charge of $+1.09$, while the tricarbonyl fragment carries a negative charge of -1.52 and the non-innocent ligand L a negative charge of -0.57. In [Mo-

$[Mo(CO)_3(phen)(H)]^{\bullet-}$

Figure 7. Calculated structure of $[Mo(CO)_3(phen)(H)]^{\bullet-}$. Atom colors: H (white), C (grey), N (blue), O (red) and Mo (green).

ChemElectroChem

Articles
doi.org/10.1002/celc.202100359

**Chemistry
Europe**
European Chemical
Societies Publishing

$[Mo(CO)_3(L)(CO_2)]^{\bullet-}$ adducts, the CO_2 ligand carries a negative charge of -0.32 which comes from both the $Mo(CO)_3$ fragment (-0.18) and the non-innocent ligand L (-0.14), as shown by the comparison with the charge distribution in $[Mo(CO)_3(L)]^{\bullet-}$. Importantly, in the CO_2 bound-ligand of $[Mo(CO)_3(L)(CO_2)]^{\bullet-}$, the two O atoms carry a negative charge, while the C atom carries a positive charge. Going from $[Mo(CO)_3(L)(CO_2)]^{\bullet-}$ to $[Mo(CO)_3(L)(COOH)]^{\bullet-}$ by protonation and reduction steps leads to a transfer of negative charges from the L ligand to the $Mo(CO)_3$ and COOH moieties by -0.28 and -0.13, respectively. A similar trends is observed when going from $[Mo(CO)_3(L)]^{\bullet-}$ to $[Mo(CO)_3(L)(H)]^{\bullet-}$, which also entails a protonation and reduction steps. This emphasizes the beneficial role of the non-innocent ligands bpy, phen and py-indz in the electrochemical activation of CO_2 and H^+. When looking at the Mulliken charge on the non-innocent ligands in the course of catalysis, the transfer of electronic density is slightly more pronounced for L = py-indz, but the discrepancy seems too small to explain a difference in reactivity between the complexes.

3. Conclusion

In summary, the studied diimine $[Mo(CO)_4(L)]$ complexes have shown similar redox properties under inert atmosphere, but somewhat different behavior in presence of carbon dioxide. In particular, low scan-rate cyclic voltammetry has revealed that reactivity with CO_2 occurs already at the mono-reduced state. Spectroelectrochemical data supported by DFT calculations suggest that the tricarbonyl $[Mo(CO)_3(L)]^{\bullet-}$ species originating from $[Mo(CO)_4(L)]^{\bullet-}$ is the key reactive species for further CO_2 activation. Two different mechanistic pathways have been identified depending on the reactivity of the tricarbonyl mono-reduced complexes with protons or carbon dioxide. Strikingly, the experimental data demonstrate that the rate of CO_2 conversion is ligand-dependent, the highest rate being obtained for the unsymmetrical py-indz Mo species.

Beyond the reactivity of the mono-reduced species towards CO_2, which remains very modest compared to other molecular metal complexes, these results fill out the idea that alternative strategies than those classically carried out for molecular electrocatalysis (i.e. donor effect of the ligand vs. redox potential) can be of high interest to enhance reactivity. In the particular case of group 6 metal carbonyl complexes, the combination of photochemistry with electrochemical methods appears as one of the most promising approach to lower the overpotential for CO_2 reduction by generating reactive species such as the putative $[Mo(CO)_3(L)]^{\bullet-}$ complex.[12e]

Experimental Section

Experimental Details

All starting materials (bipyridine, phenanthroline, $Mo(CO)_6$, KC_8) were commercially available and used as purchased, unless stated otherwise. Solvents were purified by standard methods (CaH_2 or Na/benzophenone) before use. All syntheses were conducted under

inert atmosphere of dry argon by using standard Schlenk techniques. For electrochemical and spectroelectrochemical measurements, tetrahydrofuran was passed over activated basic alumina before distillation over sodium. The solvent was collected under inert atmosphere and stored into glovebox under molecular sieves (3 Å) several days before use. The supporting salt NBu_4PF_6 was synthesized from NBu_4OH (Fluka) and HPF_6 (Aldrich). It was then purified, dried under vacuum for 48 hours at $100\,°C$, and then kept under Ar in the glovebox. Solution of THF/NBu_4PF_6 0.1 M was dried for two days over 3 Å molecular sieves before use.

Characterization Methods

Infrared spectra were recorded on a PerkinElmer Spectrum Two FTIR using a low-volume transmittance cell with CaF_2 windows from PIKE. ^1H NMR spectra were recorded at the "Services communs" of the University of Brest with a Bruker Avance 400 (400 MHz), or Bruker AMX-3 300 (300 MHz) spectrometers. All NMR data are reported in ppm (δ) relative to tetramethylsilane as external reference. Coupling constants are reported in Hertz. Electrochemical studies were performed in a glovebox (Jacomex) ($O_2 < 1$ ppm, $H_2O < 1$ ppm) with a home-made 3-electrode cell (WE: BDD or glassy carbon, RE: Pt wire in a 1 mM Fc^+/Fc THF/NBu_4PF_6 solution, CE: Pt). Ferrocene was added at the end of each experiment to determine the exact redox potential values. The potential of the cell was controlled by an AUTOLAB PGSTAT 100 (Metrohm) potentiostat monitored by the NOVA© software (Metrohm). The working electrodes were polished over a 1 μm alumina slurry with water, sonicated in H_2O (18.2 Ω.cm) and acetone, then dried with N_2 flush. Thin layer UV-Vis-NIR spectroelectrochemistry was performed with a specific home-designed cell in a reflectance mode (WE: glassy carbon or BDD, RE: Pt wire, CE: Pt wire).[25] The UV-Vis and Vis-NIR optic-fiber probes were purchased from Ocean Optics. Time-resolved UV-Vis-NIR detection was performed with a QEPro and NIRQuest spectrometers (Ocean optics). Thin layer IR spectroelectrochemistry was carried out with a home-made cell (WE: glassy carbon, RE: Pt wire, CE: Pt wire) and an ATR–Si IR optic-fiber-probe purchased from Art Photonics (ATR–P–Si-6-15-150-Lab). The WE electrode was finely modified to allow inclusion of the Si tip to achieve thin layer conditions (Figure S5). Detection of the IR signal (2 cm^{-1} resolution, one spectrum every 10 sec.) was obtained by using a FT-IR-FC model purchased from Arcoptix (FTMIR-FC-120-LN2). UV-Vis-NIR and FTIR measurements were performed in the glovebox under inert and dry atmosphere. When necessary, carbon dioxide (Alphagaz 1, Air Liquide) was introduced directly in the cell inside the glovebox by using a home-made set-up which includes a vacuum purge line. Saturation, of the THF solution with CO_2 was monitored by FTIR spectroscopy (2340 cm^{-1}). Bulk electrolysis experiments under CO_2 followed by analysis of the gaseous products by chromatography was not conducted because upon decomposition, one equivalent of Mo complex could also release up to four equivalent of CO. Accordingly, a TON value significantly larger than 4 with a faradaic efficiency of 100% must be achieved in the course of an electrolysis experiment to safely conclude to an electrocatalytic conversion of CO_2 to CO. However, the rate of the electrochemically driven reduction of CO_2 by the Mo complexes at $E_{1/2}(1)$ is modest and achieving a TON value larger than 4 will require conducting the electrolysis over a very long period of time (i.e. several hours), favoring thus the occurrence of side reactions (e.g. decomposition) that are not observed at the CV timescale.

Computational Method

All DFT calculations were performed with the Orca package (version 3.03)[26] using the PBE functional[27] and a mixed basis set (TZVP for

ChemElectroChem

Articles
doi.org/10.1002/celc.202100359

Chemistry Europe
European Chemical
Societies Publishing

H, C, N and O and LANL2DZ for Mo).[28] The calculations were accelerated with the resolution of identity (RI) approximation in conjunction with an appropriate auxiliary basis set. The geometry optimizations and frequency calculations were carried out using the conductor-like screening model (COSMO) to account for the solvation effects of THF.[29] Vibrational frequency analyses allowed us to confirm that the optimized geometries were actual minima (no imaginary frequencies) on the potential energy surface (PES) and to calculate the free energies. The calculations of the redox potentials using well established thermodynamic cycles require the use of the solvation energy of the electron in THF, which value is not known. We overcame this issue by using an internal reference and relative redox potentials. The experimental value of the reduction potential of $[Mo(CO)_4(bpy)]$ $(E_{1/2}(1)_{exp} = -1.85$ V vs. Fc$^{+/0}$) was chosen as an internal reference, and all the calculated potentials reported here are relative to that value. A difference lower than 50 mV was thus found between the calculated and experimental potentials of the $[Mo(CO)_4(phen)]^{0/\bullet-}$ and $[Mo(CO)_4(py-indz)]^{0/\bullet-}$ redox couples, which validated our approach. It is important to point out that many properties of transition metal complexes calculated by DFT are sensitive to the choice of the functional, and in particular of the amount of Hartree-Fock exchange.[30] For the systems investigated here, we found that, compared to the B3LYP hybrid functional, the PBE functional gives better agreements between calculated and experimental redox potentials, which justified our choice. Similarly, we used the estimated value of the solvation energy of H$^+$ in acetonitrile (-264.6 kcal mol^{-1}) to calculate the free energy of the protonation steps.[31] Importantly, the conductor-like screening model corresponds to a pure solution of THF ($\varepsilon = 7.25$), whereas the electrochemical measurements were carried in the presence of electrolyte at a concentration of 0.1 M in solutions saturated with CO$_2$ and, in some cases, with added water. Thus, we anticipate a large difference between the calculated and the actual values of the acidity constant of the possible intermediates. As a result, the values of the free energy of protonation reported in this work should only be compared against each other. The Avogadro software (version 1.2.0) was used to prepare the Cartesian coordinate inputs and to analyze the results.[32]

Synthetic Procedures and Characterization of the Complexes

Complexes **1**, **2** and **3** were synthesized according to reported procedures.[14a,e,33] The detailed synthesis and spectroscopic characterization of the complexes are given in the electronic supplementary information part.

Acknowledgements

Conflicts of Interest

The authors declare no conflict of interest.

[1] E. Boutin, L. Merakeb, B. Ma, B. Boudy, M. Wang, J. Bonin, E. Anxolabehere-Mallart, M. Robert, *Chem. Soc. Rev.* **2020**, *49*, 5772–5809.
[2] a) J. M. Savéant, *Chem. Rev.* **2008**, *108*, 2348–2378; b) K. E. Dalle, J. Warnan, J. J. Leung, B. Reuillard, I. S. Karmel, E. Reisner, *Chem. Rev.* **2019**, *119*, 2752–2875; c) W. Zhang, Y. Hu, L. Ma, G. Zhu, Y. Wang, X. Xue, R. Chen, S. Yang, Z. Jin, *Adv. Sci.* **2018**, *5*, 1700275; d) R. Francke, B. Schille, M. Roemelt, *Chem. Rev.* **2018**, *118*, 4631–4701.
[3] V. Kumaravel, J. Bartlett, S. C. Pillai, *ACS Energy Lett.* **2020**, *5*, 486–519.
[4] a) F. Franco, C. Rettenmaier, H. S. Jeon, B. Roldan Cuenya, *Chem. Soc. Rev.* **2020**, *49*, 6884–6946; b) C.-F. Leung, P.-Y. Ho, *Catalysts* **2019**, *9*, 760; c) C. Jiang, A. W. Nichols, C. W. Machan, *Dalton Trans.* **2019**, *48*, 9454–9468.
[5] a) M. Beley, J.-P. Collin, R. Ruppert, J.-P. Sauvage, *J. Chem. Soc. Chem. Commun.* **1984**, 1315; b) J. Collin, *Coord. Chem. Rev.* **1989**, *93*, 245–268.
[6] a) S. Meshitsuka, M. Ichikawa, K. Tamaru, *J. Chem. Soc. Chem. Commun.* **1974**, 158; b) C. M. Lieber, N. S. Lewis, *J. Am. Chem. Soc.* **1984**, *106*, 5033–5034.
[7] a) J. Hawecker, J.-M. Lehn, R. Ziessel, *J. Chem. Soc. Chem. Commun.* **1984**, 328–330; b) J. Hawecker, J.-M. Lehn, R. Ziessel, *Helv. Chim. Acta* **1986**, *69*, 1990–2012.
[8] C. M. Bolinger, N. Story, B. P. Sullivan, T. J. Meyer, *Inorg. Chem.* **2002**, *27*, 4582–4587.
[9] a) M. Bourrez, F. Molton, S. Chardon-Noblat, A. Deronzier, *Angew. Chem. Int. Ed.* **2011**, *50*, 9903–9906; *Angew. Chem.* **2011**, *123*, 10077–10080; b) M. D. Sampson, C. P. Kubiak, *J. Am. Chem. Soc.* **2016**, *138*, 1386–1393.
[10] a) M. Hammouche, D. Lexa, J. M. Savéant, M. Momenteau, *J. Electroanal. Chem.* **1988**, *249*, 347–351; b) C. Costentin, S. Drouet, G. Passard, M. Robert, J. M. Savéant, *J. Am. Chem. Soc.* **2013**, *135*, 9023–9031; c) C. Costentin, G. Passard, M. Robert, J. M. Savéant, *Proc. Natl. Acad. Sci. USA* **2014**, *111*, 14990–14994; d) J. Bonin, A. Maurin, M. Robert, *Coord. Chem. Rev.* **2017**, *334*, 184–198.
[11] a) L. Rotundo, J. Filippi, R. Gobetto, H. A. Miller, R. Rocca, C. Nervi, F. Vizza, *Chem. Commun.* **2019**, *55*, 775–777; b) B. Reuillard, K. H. Ly, T. E. Rosser, M. F. Kuehnel, I. Zebger, E. Reisner, *J. Am. Chem. Soc.* **2017**, *139*, 14425–14435; c) S. Sato, K. Saita, K. Sekizawa, S. Maeda, T. Morikawa, *ACS Catal.* **2018**, *8*, 4452–4458; d) A. Maurin, M. Robert, *J. Am. Chem. Soc.* **2016**, *138*, 2492–2495; e) J. Choi, J. Kim, P. Wagner, S. Gambhir, R. Jalili, S. Byun, S. Sayyar, Y. M. Lee, D. R. MacFarlane, G. G. Wallace, D. L. Officer, *Energy Environ. Sci.* **2019**, *12*, 747–755.
[12] a) S. L. Hooe, J. M. Dressel, D. A. Dickie, C. W. Machan, *ACS Catal.* **2019**, *10*, 1146–1151; b) J. O. Taylor, F. L. P. Veenstra, A. M. Chippindale, M. J. Calhorda, F. Hartl, *Organometallics* **2018**, *38*, 1372–1390; c) F. Franco, C. Cometto, F. Sordello, C. Minero, L. Nencini, J. Fiedler, R. Gobetto, C. Nervi, *ChemElectroChem* **2015**, *2*, 1372–1379; d) P. Zhang, X. Yang, X. Hou, X. Xu, B. Xiao, J. Huang, C. Stampfl, *Phys. Chem. Chem. Phys.* **2019**, *21*, 23742–23748; e) J. O. Taylor, Y. Wang, F. Hartl, *ChemCatChem* **2019**, *12*, 386–393; f) D. Sieh, D. C. Lacy, J. C. Peters, C. P. Kubiak, *Chem. Eur. J.* **2015**, *21*, 8497–8503; g) L. Rotundo, C. Garino, R. Gobetto, C. Nervi, *Inorg. Chim. Acta* **2018**, *470*, 373–378; h) K. A. Grice, C. Saucedo, *Inorg. Chem.* **2016**, *55*, 6240–6246; i) K. A. Grice, *Coord. Chem. Rev.* **2017**, *336*, 78–95; j) G. Neri, P. M. Donaldson, A. J. Cowan, *J. Am. Chem. Soc.* **2017**, *139*, 13791–13797; k) M. L. Clark, K. A. Grice, C. E. Moore, A. L. Rheingold, C. P. Kubiak, *Chem. Sci.* **2014**, *5*, 1894–1900; l) J. O. Taylor, R. D. Leavey, F. Hartl, *ChemElectroChem* **2018**, *5*, 3155–3161; m) J. Tory, B. Setterfield-Price, R. A. W. Dryfe, F. Hartl, *ChemElectroChem* **2015**, *2*, 213–217.
[13] a) R. Hille, J. Hall, P. Basu, *Chem. Rev.* **2014**, *114*, 3963–4038; b) A. C. Ghosh, C. Duboc, M. Gennari, *Coord. Chem. Rev.* **2021**, *428*, 213606.
[14] a) C. M. Álvarez, L. Álvarez-Miguel, R. García-Rodríguez, J. M. Martín-Álvarez, D. Miguel, *Eur. J. Inorg. Chem.* **2015**, *2015*, 4921–4934; b) S. L. Mukerjee, S. P. Nolan, C. D. Hoff, R. Lopez de la Vega, *Inorg. Chem.* **2002**, *27*, 81–85; c) A. Vlček Jr, *Coord. Chem. Rev.* **2002**, *230*, 225–242; d) H. J. Bruins Slot, N. W. Murrall, A. J. Welch, *Acta Crystallogr.* **1985**, *41*, 1309–1312; e) M. H. B. Stiddard, *J. Chem. Soc.* **1962**, 4712–4715; f) S. S. Braga, A. C. Coelho, I. S. Gonçalves, F. A. Almeida Paz, *Acta Crystallogr.* **2007**, *63*, m780–m782.
[15] T. S. A. Hor, S.-M. Chee, *J. Organomet. Chem.* **1987**, *331*, 23–28.
[16] a) J. A. Connor, C. Overton, *J. Organomet. Chem.* **1983**, *249*, 165–174; b) R. Johnson, H. Madhani, J. P. Bullock, *Inorg. Chim. Acta* **2007**, *360*, 3414–3423.
[17] L. Yang, J. K. Feng, A. M. Ren, *Synth. Met.* **2005**, *152*, 265–268.

[18] a) D. Miholová, A. A. Vlček, *J. Organomet. Chem.* **1985**, *279*, 317–326; b) D. Miholová, B. Gaš, S. Záliš, J. Klíma, A. A. Vlček, *J. Organomet. Chem.* **1987**, *330*, 75–84.

[19] J. A. Vlček, F. Baumann, W. Kaim, F.-W. Grevels, F. Hartl, *J. Chem. Soc. Dalton Trans.* **1998**, 215–220.

[20] T. Bens, P. Boden, P. Di Martino-Fumo, J. Beerhues, U. Albold, S. Sobottka, N. I. Neuman, M. Gerhards, B. Sarkar, *Inorg. Chem.* **2020**, *59*, 15504–15513.

[21] J.-M. Savéant, *Elements of molecular and biomolecular electrochemistry*, John Wiley & Sons **2006**.

[22] a) J. D. Froehlich, C. P. Kubiak, *J. Am. Chem. Soc.* **2015**, *137*, 3565–3573; b) F. Franco, C. Cometto, L. Nencini, C. Barolo, F. Sordello, C. Minero, J. Fiedler, M. Robert, R. Gobetto, C. Nervi, *Chem. Eur. J.* **2017**, *23*, 4782–4793.

[23] A. L. Ostericher, T. M. Porter, M. H. Reineke, C. P. Kubiak, *Dalton Trans.* **2019**, *48*, 15841–15848.

[24] C. Costentin, S. Drouet, M. Robert, J. M. Savéant, *Science* **2012**, *338*, 90–94.

[25] a) I. Lopez, R. Cao, D. A. Quist, K. D. Karlin, N. Le Poul, *Chem. Eur. J.* **2017**, *23*, 18314–18319; b) A. Thibon-Pourret, F. Gennarini, R. David, J. A. Isaac, I. Lopez, G. Gellon, F. Molton, L. Wojcik, C. Philouze, D. Flot, Y. Le Mest, M. Reglier, N. Le Poul, H. Jamet, C. Belle, *Inorg. Chem.* **2018**, *57*, 12364–12375.

[26] F. Neese, *WIREs Comput. Mol. Sci.* **2011**, *2*, 73–78.

[27] J. P. Perdew, K. Burke, M. Ernzerhof, *Phys. Rev. Lett.* **1996**, *77*, 3865–3868.

[28] a) A. Schäfer, H. Horn, R. Ahlrichs, *J. Chem. Phys.* **1992**, *97*, 2571–2577; b) P. J. Hay, W. R. Wadt, *J. Chem. Phys.* **1985**, *82*, 270–283.

[29] A. Klamt, G. Schüürmann, *J. Chem. Soc. Perkin Trans. 2* **1993**, 799–805.

[30] K. A. Moltved, K. P. Kepp, *J. Chem. Theory Comput.* **2018**, *14*, 3479–3492.

[31] C. P. Kelly, C. J. Cramer, D. G. Truhlar, *J. Phys. Chem. B* **2007**, *111*, 408–422.

[32] M. D. Hanwell, D. E. Curtis, D. C. Lonie, T. Vandermeersch, E. Zurek, G. R. Hutchison, *J. Cheminf.* **2012**, *4*, 17.

[33] G. A. Ardizzoia, M. Bea, S. Brenna, B. Therrien, *Eur. J. Inorg. Chem.* **2016**, *2016*, 3829–3837.